JOURNAL OF MAGNETIC RESONANCE **126,** 87–94 (1997)
ARTICLE NO. MN971138

ESR Study of Electron–Nuclear Dipolar Relaxation for AsO_4^{4-} Spin Probe in the Paraelectric Phase of KH_2AsO_4

B. Rakvin and D. Merunka

Ruder Bošković Institute, P.O. Box 1016, 10001 Zagreb, Croatia

Received December 9, 1996

Saturation behavior of allowed and forbidden ESR transition of AsO_4^{4-} paramagnetic probe in KH_2AsO_4 was studied in the wide temperature interval around the paraelectric–ferroelectric phase transition, T_c. The ratios between forbidden and allowed line intensities were employed to deduce information on the electron–nuclear dipolar (END) relaxation mechanism. It was shown that a proton END relaxation mechanism exhibits an extremal temperature behavior in the paraelectric phase around 230 K. The extremal temperature behavior was described by employing a model of proton hopping along the O–H···O bonds around the paramagnetic centers, and the correlation time of this hopping was estimated in the wide temperature range in the paraelectric phase (150–330 K). The temperature dependence of effective proton distance from the neighbor oxygens was obtained, and it was discussed in terms of a localization of the spin density on these oxygens caused by charge inbalance in the As–O bonds in the ferroelectric phase.

INTRODUCTION

The paramagnetic center AsO_4^{4-} has been extensively studied in KH_2AsO_4 (KDA) and in other KH_2PO_4 (KDP)-type ferroelectrics (*1, 2*). This center was employed as a probe to study slow lattice dynamics and slow polarization fluctuations (10^7–10^{10} Hz) in the vicinity of the paraelectric–ferroelectric phase transition temperature, T_C. For KDP-type ferroelectrics containing AsO_4^{4-} and SeO_4^{3-} probes, Weisensee *et al.* (*3*) and Poole *et al.* (*4*) demonstrate that the electron spin–lattice relaxation time, T_1, passing through the phase transition exhibits an anomalous behavior at T_C, showing that the probe couples to the critical modes. This anomalous behavior of T_1 has been described by different theoretical models (*3, 4*). Moreover, T_1 detected in the much wider temperature range (2–200 K) has been also described with different relaxation mechanisms, a two-phonon Raman process involving acoustical and optical phonons for the KDA:AsO_4^{4-} system (*3*) and only a two-phonon Raman process for the KDP:SeO_4^{3-} system (*4*), respectively. It is interesting to note that the magnitude of the Debye temperature, Θ_D, obtained from these analyses (*3, 4*) (~90 K) was smaller by a factor of three from that (~287 K) estimated from specific heat measurements (*5*). However, more recent ESR and ENDOR studies on several KDP-type lattices were performed, and an additional reaxation mechanism due to an exponential broadening effect was noted (*6–8*). Furthermore, the clear evidence that this exponential relaxation rate exhibits the same activation energy as the activation energy for the local polarization fluctuation means that the microscopic origin for the exponential type of relaxation rate is not quite clear (*6–8*). Therefore, it can be concluded that all these discrepancies reflect an uncertainty in a microscopic mechanism responsible for the T_1 process.

Concerning the T_1 data in the KDA lattice, any attempt to fit these data with larger values of Θ_D leads to large deviation of calculated data (*9*) from the reported experimental measurements (*3, 4*). It can be supposed that a Θ_D evaluated from the Raman relaxation mechanism is smaller than Θ_D obtained from specific heat, because explanations of Raman relaxation processes are usually restricted to acoustic vibrations. Since the specific heat of a KDP type of lattice exhibits a large maximum in c/T^3 around 20 K, the Einstein density of states was used to approximate the optical-phonon part of the phonon spectrum (*5, 10*). The Einstein mode in the KDP type of lattice is assigned as a residual soft mode, and the origin of this mode is associated with low-lying hydrogen modes. This consideration suggests that an additional relaxation mechanism (*9, 11*) (based on electron–nuclear dipolar interaction, END) which is closely related to the proton dynamics in the KDP type of lattice can be also involved in the spin–lattice relaxation rate of the AsO_4^{4-} paramagnetic center. Moreover, this assumption has been also motivated by the well-known fact that hydrogen motion plays an essential role in two different models [tunneling model (*12, 13*) and order–disorder model (*14*)] which have been proposed for the description of a ferroelectric phase transition in the KDP-type compounds.

An additional problem is that a modulation of the hyperfine coupling constant is usually much less effective than the modulation of spin-orbit coupling, and in such cases, a significant contribution to the relaxation rate is not expected

1090-7807/97 $25.00

(*11*). However, fluctuations of the environment of the paramagnetic probe, for example protons in KDP, can strongly affect the nuclear spin–lattice relaxation time of the nuclei. In the following case when electron- and nuclear-spin fluctuations are mixed, the two relaxation rates are combined, and forbidden ESR transitions ($\Delta M_S = \pm 1$, $\Delta M_I = \pm 1$) became partially allowed (*15*). Therefore, one expects that a cross-relaxation rate affects T_1 in a coupled electron–proton system providing important information on proton dynamics in the vicinity of the probe (*16–18*).

This paper describes our effort to obtain additional experimental evidence for the examination of the possible role of an END relaxation mechanism in the relaxation rate of the AsO_4^{4-} paramagnetic center in the KDA lattice. Simultaneous spin-flip transitions ($\Delta M_S = \pm 1$, $\Delta M_I = \pm 1$) and their saturation behavior have not been studied in detail for a typical paramagnetic probe (AsO_4^{4-}, SeO_4^{3-}, or CrO_4^{3-}) in the KDP type of lattice. Such a study could provide important information leading to a more complete and reliable relaxation model. The resulting END relaxation parameters can serve to provide a better understanding of the role of hydrogen dynamics in the hydrogen-bonding ferroelectrics. In order to obtain this evidence, we have studied saturation behavior of the spin-flip and ESR transitions for the AsO_4^{4-} center in a wide temperature interval, 77–330 K.

EXPERIMENTAL

Single crystals of KH_2AsO_4 were grown from saturated aqueous solution by slow evaporation. The AsO_4^{4-} probe was formed by gamma irradiating the crystals with a dose of about 0.5 kG (not critical) at room temperature. All ESR measurements were made with a Varian E9 (X band) spectrometer. The sample temperature was controlled by a Bruker digital temperature controller, Model ER4111VT. A PC computer was used for the data acquisition and lineshape simulation.

EXPERIMENTAL RESULTS

Spectroscopic Characteristics of AsO_4^{4-} in KH_2AsO_4

A typical ESR spectrum of this probe in the KDA lattice at room temperature consists of four main peaks separated by about 100 mT due to hyperfine interaction with the ^{75}As ($I = \frac{3}{2}$) nuclei (*1, 2, 19–22*). Each ^{75}As hyperfine peak was found to split into a 1:4:6:4:1 quintet due to equal superhyperfine interaction with the four O–H$\cdots$O protons. An earlier ESR study by Blinc *et al.* (*19*) demonstrated that the 1:4:6:4:1 quintet had changed to a 1:2:1 triplet at the temperature of 220 K (T^*). This temperature is significantly higher than the paraelectric–ferroelectric transition temperature ($T_C = 97$ K) for KDA, because of the freezing of proton lattice fluctuations around the probe (which is a defect with excess charge, $1e^-$) on the ESR time scale of 10^{-8}–10^{-10} s in comparison to the proton dynamics of the unirradiated lattice. In earlier studies (*19, 20, 22*), it was suggested that the probe exhibits a local type of dynamics on the ESR time scale. The local behavior of the probe has been attributed to the transformation from the high (paraelectric) to the low (ferroelectric) symmetry ESR spectra at temperature T^*. By employing modified Bloch equations, such a phenomenon can be used for obtaining the low-frequency molecular fluctuations in the KDP type of solids in the temperature region around T^*. The fluctuations obtained has been described with a simple Arrhenius-type correlation time $\tau = \tau_0 \exp(\Delta E/KT)$ in some reports (*19, 21, 22*), but with a non-Arrhenius behavior in other studies (*23, 24*). A deviation from an Arrhenius law is interpreted by employing the theoretical model which predicts a local motional freezing of the spin probe in the paraelectric phase. According to the model (*23, 24*), activation energy, ΔE, for the probe should increase as $[a - b(T - T_C)^{1/2}]$ as $T \rightarrow T_C$ with $a > b$. Recently, it has been shown that some of the non-Arrhenius behavior can be ascribed to the omission of at least two processes: (a) a line-broadening process which depends exponentially on the temperature (*6–8*); and (b) inhomogeneous broadening due to proton spin-flip transitions (*25*). By employing ESR (*6, 7, 25*) and ENDOR (*8*) techniques, this was indeed found to be true for KDA and KDP:AsO_4^{4-} systems where ΔE is essentially temperature independent down to T_C.

Forbidden ESR Transitions and the END Relaxation Mechanism

As mentioned above (*25*), a detailed consideration of proton spin-flip transitions in AsO_4^{4-} KDA helps us to minimize the error due to the line-broadening mechanisms in the calculation of τ for AsO_4^{4-} center. It is well known (*15*) that a detected satellite line represents a so-called ''forbidden ESR transition'' and gives us information on NMR proton transitions on the ESR scale. By comparison between the intensity of the main ESR transition and the intensity of the spin-flip transition, one can estimate alternative information about proton coupling to the paramagnetic center. For example, for the randomly oriented protons around the paramagnetic center, the ratio between intensity of the satellite line (I_s) and the intensity of the main line (I_m) can be employed for calculation of an effective single-proton distance, r_{ef}, as given by Poole and Farach (*15*):

$$\frac{I_s}{I_m} = \frac{3}{10}\left(\frac{g\beta}{Hr_{ef}^3}\right)^2;\ r_{ef} = \left(\left\langle \sum_j \frac{1}{r_j^6} \right\rangle\right)^{-1/6}, \qquad [1]$$

where g is the electronic gyromagnetic ratio and β is electronic magnetic moment. In a similar way, this ratio can be used to obtain information on a spin-relaxation process from

the differential saturation factor of the main and satellites lines as was suggested by Shimizu (*18*). As a model to calculate the relaxation rates for the ESR transition and for the spin-flip transition Shimizu (*18*) employed a paramagnetic center (C–H fragment) containing an unpaired electron in the $2p_z$ orbital in a crystal lattice. The two spins are described with the four energy levels (I, II, III, and IV) which define two transition probabilities for ESR (IV $\rightarrow$ II and III $\rightarrow$ I) as (*18*)

$$W_{ij} = w(T)\cos^2(\theta + \theta') \qquad [2]$$

and the other two, for the spin-flip transitions (III $\rightarrow$ II and IV $\rightarrow$ I), as (*18*)

$$W_{ij} = w(T)\sin^2(\theta + \theta'), \qquad [3]$$

where θ and θ' are proportional to mixing elements of the proton hyperfine tensor and $w(T)$ is a temperature-dependent transition probability containing all other mechanisms which are coupled over the spin-orbit coupling to the lattice. Probabilities for the nuclear transition (II $\rightarrow$ I and IV $\rightarrow$ III) are neglected. After evaluation of the saturation factors for the two ESR and for the two spin-flip transitions, the intensity ratio I_s/I_m has been obtained as (*18*)

$$\frac{(I_s/I_m)}{(I_s/I_m)_0} = \frac{1 + G_m P}{1 + G_s P} \qquad [4]$$

with the parameters G_m and G_s

$$G_m = \left(\frac{g\beta}{2\hbar}\right)^2 f(0) k \frac{1}{c} \cos^2(\theta + \theta')\Omega_m \qquad [5]$$

$$G_s = \left(\frac{g\beta}{2\hbar}\right)^2 f(0) k \frac{1}{c} \sin^2(\theta + \theta')\Omega_s \qquad [6]$$

$$\Omega_m = \frac{1 + \cos^2(\theta + \theta')}{2w \cos^2(\theta + \theta')} \qquad [7]$$

$$\Omega_s = \frac{1 + \sin^2(\theta + \theta')}{2w \sin^2(\theta + \theta')}, \qquad [8]$$

where $f(0)$ represents a spectral lineshape, k is a proportionality constant between observed intensity and transition frequency for a component line, c is a constant of proportionality between the amplitude of the microwave magnetic field and microwave power, and Ω represents the effective spin–lattice relaxation for one of the transitions. It has also been shown (*18*) that in the limiting case of weak mixing [$\sin^2(\theta + \theta') \ll 1$], for $P \rightarrow 0$, $(I_s/I_m)_0 = tg^2(\theta + \theta')$, and for $P \rightarrow \infty$, $(I_s/I_m)_\infty = (\Omega_m/\Omega_g) = 2tg^2(\theta + \theta')$, the intensity ratio is

$$\frac{(I_s/I_m)_\infty}{(I_s/I_m)_0} = 2. \qquad [9]$$

In the weak-mixing limit where I_s is much weaker than I_m, the saturation of the two lines is comparable at small microwave power. Moreover, this ratio changes only by a factor of two even in the limit when $P \rightarrow \infty$. Shimizu also shows (*18*) that, if an intramolecular dipolar interaction is modulated by molecular dynamics (or proton dynamics), the saturation factors for I_s are much larger than those for I_m and $(I_s/I_m)/(I_s/I_m)_0$ can increase more than a factor of 2. Thus, analysis of the saturation behavior for I_s/I_m can provide information on the relevance of an END mechanism to the relaxation rate of a paramagnetic center.

Saturation Measurements for Allowed and Forbidden ESR Transitions in KH_2AsO_4:AsO_4^{4-}

The required experimental condition which is suitable for this type of relaxation study assumes that satellite lines are well resolved from the main line. There are two limiting factors which usually cause difficulties to detect a well-resolved spin-flip transition. In the region of high magnetic field, these lines exhibit satisfactory splitting (larger than the linewidth of the main line) but with the intensities of the lines becoming much smaller than the intensity of the main ESR line. On the other hand, at lower magnetic field, the intensity of the satellite line increases but its separation is not usually larger than the linewidth of the main line.

Clear evidence for the occurrence of the nuclear spin-flip ($\Delta M_S = \pm 1$, $\Delta M_I = \pm 1$) transitions for AsO_4^{4-} center can be easily noted around the fourth ($M_I = -\frac{3}{2}$) hyperfine line at 465 mT, taking the crystal orientation along the minimum proton hyperfine interaction in the *ab* plane, as shown in Fig. 1a. This line contains well-resolved satellites which exhibit splitting of $\sim 2g_n\beta_n H$ (1.42 mT at $H = 465$ mT) for protons. As can be noted, the splitting between the satellites can be easily checked for each arsenic hyperfine line because of the large difference in the position of each hyperfine line (from 100 to 460 mT). The more detailed assignments of these satellites have been provided earlier (*25*). It is important to note that we will focus on only the ($M_I = -\frac{3}{2}$) arsenic line, which does not exhibit detectable splitting as do other arsenic lines at lower magnetic field on passing through T^*. The width of this line is nearly constant in the wide temperature interval exhibiting a small change around 220 K. This inhomogeneous line together with satellites can be well described by a simple composite of the three Gaussian profiles in the high-temperature regime ($T > 220$ K). It is worth noting that the same linewidth of the Gaussian lineshape describes the main and the satellite lines.

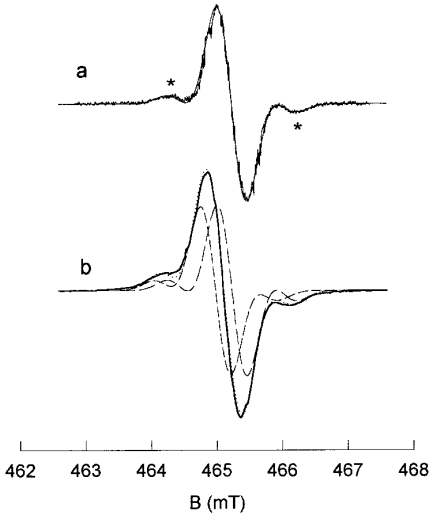

FIG. 1. A typical ($M_I = -\frac{3}{2}$) ESR line from the AsO_4^{4-} center in KDA. The well-resolved satellites from both sides of the main line with a splitting of 1.42 mT are indicated by asterisks. The spectrum (a) obtained at 300 K is fitted with a composite Gaussian lineshape containing three Gaussians, one for the main line and two for satellites lines, with the same linewidth ($\Delta_{pp} = 0.46$ mT) for all the lineshapes. The spectrum (b) obtained at 230 K is described by two composite Gaussian lineshapes represented by dashed lines and the composite spectrum represented by the dotted line. The splitting between the two composite Gaussian lines is smaller (0.25 mT) than the width Δ_{pp}.

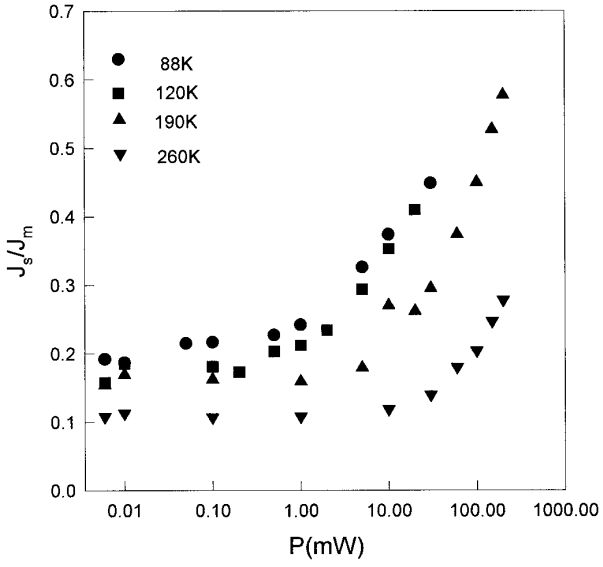

FIG. 2. Microwave saturation dependence of the ratio (J_s/J_m) at several characteristic temperatures, where J_s corresponds to the intensity of a satellite line and J_m to the intensity of the main line, respectively.

The broadening of the spectrum and small asymmetry contribution which appeared in the low-temperature region ($T < 220$ K) can be approximated with the two nearly identical composite Gaussian lineshapes whose total linewidth is larger than the splitting between these lines as shown in Fig. 1b. Thus, in the low-temperature region, one can assume that the ($M_I = -\frac{3}{2}$) line also splits (as well as other arsenic lines), but with a splitting which is smaller than the linewidth of ($M_I = -\frac{3}{2}$) line. Taking into account the crystal orientation in the magnetic field and the tensor data deduced earlier (*20*), the splitting noted corresponds to the different local domains while the hyperfine proton splitting (nearby proton) remained unchanged. This approximate description of the lineshape helps us to evaluate the intensity of the main line, J_m, as well as the intensity of satellite line, J_s, more accurately in a wide temperature interval around T^*.

The microwave saturation effects of the ($M_I = -\frac{3}{2}$) arsenic line with its corresponding satellites have been studied in the temperature interval 77–300 K. The change of J_s/J_m as a function of microwave power is shown in Fig. 2 at several characteristic temperatures. The values of J_s/J_m obtained for different temperatures in the limit of small microwave power can be seen on an enlarged scale in Fig. 3. The observed values exhibit the expected temperature behavior according to Eq. [1] where an effective distance between AsO_4^{4-} center and protons, r_{ef}, decreases with decreasing temperature. Since in the region for $P \sim 0$, J_s/J_m exhibits different values at different temperatures, it is convenient to apply a scaling procedure by employing Eq. [4]. Figure 4 represents data in the form where all saturation-dependent data measured at one temperature are normalized to residual values $(J_s/J_m)_0$ for $P \to 0$. It should be noted here that this type of scaling helps us to avoid uncertainty in the intensity of the main line. As was mentioned above, the most convenient orientation is

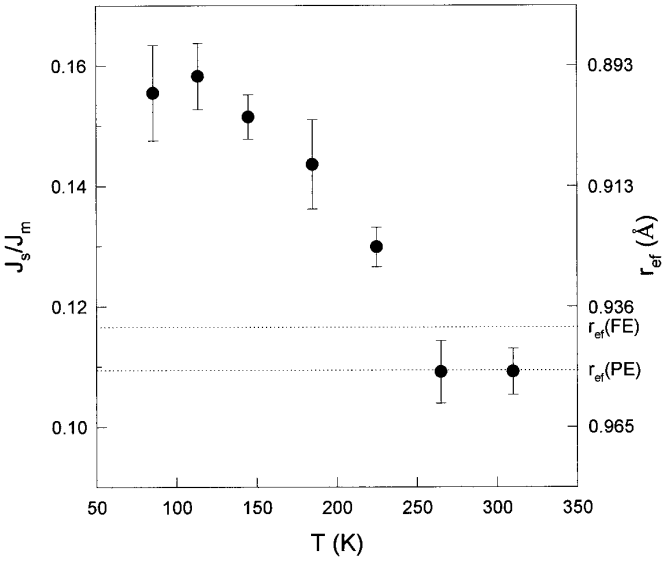

FIG. 3. Temperature dependence of the ratio (J_s/J_m) measured at 0.01 mW of microwave power. The parameter of effective proton distance, r_{ef}, obtained from Eq. [1] for the paraelectric phase, is shown on the right ordinate axis.

in the direction of minimum mixing, where the two ESR transitions give an intense central line containing a weak-intensity spin-flip transition on each side of the central line. In addition, by taking normalized data one expects that possible effects of multispin systems (four equivalent protons) will be reduced (*15*). Thus, the normalized ratio of the experimentally measured intensities will be employed as an approximative normalized ratio $(J_s/J_m)/(J_s/J_m)_0 \approx (I_s/I_m)/(I_s/I_m)_0$.

It can be noted that all $(J_s/J_m)/(J_s/J_m)_0$ obtained at high temperatures (330 K) fall below 2, while for some lower temperatures these ratios become larger than 2. According to the Shimizu model (*18*), a ratio larger than 2 can be considered as an anomalous saturation behavior and can be explained by introducing an additional END relaxation mechanism. Thus, the data obtained clearly demonstrate that END relaxation mechanism also contributes to the total relaxation rate for the AsO_4^{4-} paramagnetic center in KDA. The maximum contribution of this mechanism is expected around (220 K) where the largest anomalous saturation has been detected. In order to analyze this anomalous saturation behavior, G values were deduced by fitting saturation data (Fig. 4) to Eq. [4] at different temperatures. Evaluated data for G_m and G_s as a function of temperature as well as their ratio are shown in Fig. 5. From these results, two important features in the temperature behavior of these parameters can be noted. Since the effective spin–lattice relaxation time is proportional to G, the temperature dependence should reflect the change in effective relaxation time. One notes an unusual behavior whereby the G_s decreases with decrease in temperature (from 330 to 220 K) and in the lower-temperature region reaches the expected behavior; then it increases with further decrease in temperature (from 220 K to 150 K). The second feature can also be noted in Fig. 5 where the ratio

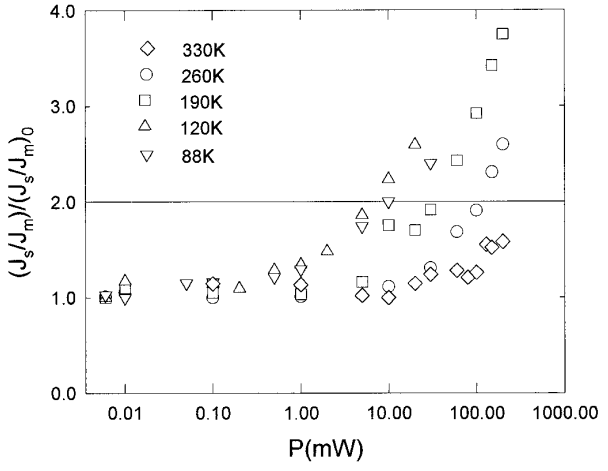

FIG. 4. Microwave saturation dependence of $(J_s/J_m)/(J_s/J_m)_0$ at several characteristic temperatures. The value of $(J_s/J_m)_0$ is evaluated in the limit when $P \to 0$ from Fig. 2.

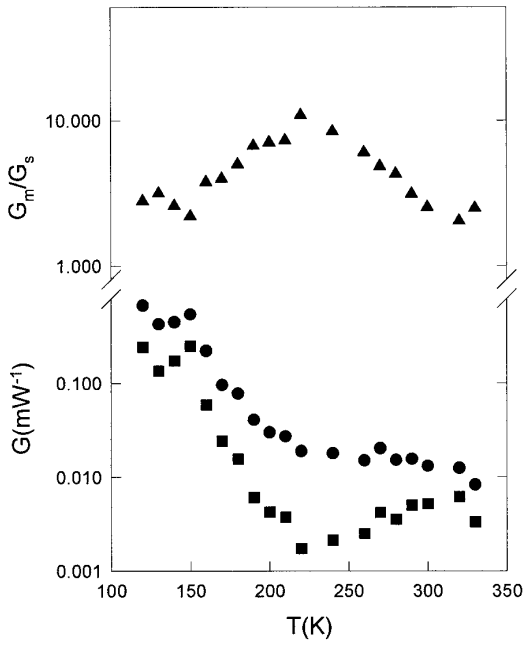

FIG. 5. Temperature dependence of parameters G_s (squares), G_m (circles), and G_m/G_s (triangles) obtained by fitting Eq. [4] to the experimental results as presented in Fig. 4.

of these parameters exhibits clear extreme behavior for the monitored temperature interval, and moreover, the value of the ratio is five times larger than the expected maximum value as given in Eq. [9].

DISCUSSION

Proton Localization along the O–H···O Bond

One notes that an effective proton distance usually can be evaluated directly from hyperfine tensor data, but this approach requires a much longer procedure for obtaining tensor elements at different temperatures. In further analysis of (J_s/J_m) and its temperature behavior, it is convenient to estimate a proportionality constant (in Eq. [1]) for our particular crystal orientation in order to discuss the temperature dependence of r_{ef}. One expects that the most convenient temperature region to estimate the constant of proportionality is in the paraelectric phase, since in this phase, all four protons are equally coupled to the nearest oxygen. By employing r_{OH} values[1] (*26*) and Eq. [1], the effective proton distance in the paraelectric phase $r_{ef}(PE) = 0.951$ Å, and the constant of proportionality is obtained. The temperature dependence of r_{ef}, calculated from the proportionality constant, is shown on the right ordinate axis in Fig. 3. In the

[1] The structural parameters obtained by high-resolution neutron-diffraction data for isomorphous lattice KH_2PO_4 were employed to describe vicinity of the AsO_4^{4-} paramagnetic center in the ferroelectric phase (*27*).

ferroelectric phase (see Footnote 1), the $r_{ef}(FE) = 0.941$ Å is calculated by employing two nearby protons at $r_{OH} = 1.056$ Å and two more distant protons at $r_{OH} = 1.441$ Å. It can be noted that the obtained $r_{ef}(FE) = 0.941$ Å as indicated by the dashed line in Fig. 3 is significantly larger than the expected $r_{ef}(FE) \sim 0.89$ Å in the ferroelectric phase. One of the possible explanations for this discrepancy leads to a closer localization of the nearby proton to the neighboring nearby oxygen. For example, to reach $r_{ef}(FE) \sim 0.89$ Å, one should employ an unrealisticly small $r_{OH} = 1.001$ Å. Another possible model which can be employed to describe J_s/J_m in the ferroelectric phase should involve an additional change of spin density on the nearby oxygen. In recent experimental and theoretical studies (*28, 29*) of the proton hyperfine splitting tensors and corresponding spin densities for AsO_4^{4-} and SeO_4^{3-} paramagnetic centers in the ferroelectric phase, it was shown that spin density significantly increases on the oxygen near the nearby proton (0.3) in comparison to spin density on the oxygen near the more distant proton (0.05), while in the paraelectric phase the spin density is equal for all four oxygens (0.18). Moreover, it was shown that because of such a density distribution in the ferroelectric phase the dipolar interaction along the $r(O_{close}-H_{far}) \sim 2.6$ Å direction is stronger than the dipolar interaction along $r(O_{far}-H_{far}) \sim 1.4$ Å, and besides, the distance in the last case is significantly smaller (*29*). Taking into account the increase of spin density on the nearby oxygen of about 40% in the ferroelectric phase, as was predicted by the above model (*28, 29*), $J_s/J_m = 0.163$ is calculated. The estimated ratio coincides with the experimentally obtained data ($J_s/J_m = 0.158 \pm 0.009$) as can be seen in Fig. 3. This agreement provides additional support for the model proposed earlier (*28, 29*) of spin distribution in the ferroelectric phase which has the important implication that the spontaneous polarization of the KDP type of compounds originates from charge imbalance in the P–O (As–O) bonds caused by proton localization rather than from the relative displacement of the K and P (As) atoms.

Proton Dynamics and END Relaxation Rates

As was mentioned above, the saturation behavior of (I_s/I_m) can be associated with an additional modulation of the hyperfine interaction due to proton motions in the temperature interval examined. The results seem to suggest that for the AsO_4^{4-} center in KDA, proton hopping in an asymmetric double-well potential along a O–H···O bond modulates a dipolar hyperfine interaction and produces anomalous behavior of the saturation parameters. In the case of KDA, it is not convenient to apply earlier considerations (*18*) for the description of the anomalous saturation behavior, because in that case the dipolar interaction was modulated by a torsional oscillation of the molecule. Contribution of END relaxation which is modulated by the more appropriate hopping motion (τ) was discussed earlier (*16*), and here only a qualitative description will be used. The model (*16*) is based on the assumptions that the fluctuation amplitude of the hopping process at the distance between spins, r, is larger than the angular fluctuation involving the angle, ϕ, between the magnetic field and the direction along r. It can be noted (*16*) that the lattice-induced transition probabilities for END are proportional to Δr^{-6} (hopping distance) and can be incorporated to the transition probabilities for the two-spin system as defined in Eq. [2] and Eq. [3]. The new transition probabilities will include induced transition probabilities between nuclear states and additional terms for transition probabilities of the main and satellite lines. The temperature-dependent part of these transitions which leads to extreme behavior is proportional to functional form (*11*)

$$W_{\mu\nu} \sim \frac{\tau}{1 + (\omega_{\mu\nu}\tau)^2}, \qquad [10]$$

where $\omega_{\mu\nu}$ corresponds to an electron or a nuclear transition energy and can be replaced with the electron or nuclear Larmor frequency, and τ is the correlation time of proton hopping.

According to Eq. [10], the transition probability for the main and satellite lines reaches a maximum when the relaxation rate reaches a value of $1/\tau \approx \omega_e$, while for the nuclear transition the maximum appears at $1/\tau \approx \omega_n$. To further check the mechanism suggested above, one can use previously obtained (*21, 22, 25*) τ values, which describe proton dynamics, in order to elucidate possible relaxation mechanism more accurately. Therefore, one calculates the temperature of the extreme relaxation time for these two mechanisms and finds that for $\omega_e = 59.7$ GHz the maximum of the transition probability can be expected at around 590 K. On the other hand, taking a nuclear Larmor frequency of 124 MHz, the maximum relaxation rate is obtained at 230 K. Since this temperature almost coincides with the temperature at which the maximum of G_s/G_m is found, it can be supposed that term with the nuclear relaxation rate should be responsible for this extreme behavior. On the other hand, similar terms containing electron Larmor frequencies can be neglected for this slow proton hopping ($\tau\omega_e \gg 1$). According to this finding, besides the previously defined transitions for the main and satellite lines given in Eq. [2] and Eq. [3], new nuclear transition probabilities (II → I and IV → III) will now be included in the system of the two spins. These nuclear transition probabilities are given in the form (*16*)

$$W_n = h(T) \sim \frac{9}{16}\frac{(g_e\beta_e g_n\beta_n h^2)^2 \sin^2\phi\cos^2\phi}{\Delta r^{-6}}\frac{\tau}{1 + (\omega_n\tau)^2}. \qquad [11]$$

By using Eq. [2], Eq. [3], and Eq. [4], a new effective relaxation time for the main and satellite lines is calculated in order to describe the anomalous behavior of G_s/G_m. Effective relaxation times for the main and satellite lines are obtained by considering the network of relaxation paths as a network of resistances, and in the limit of weak mixing,

$$\Omega_m = \frac{1}{w(T)\cos^2(\theta + \theta')} \qquad [12]$$

and for satellite lines taking additional approximation, $w + h \approx w$:

$$\Omega_s = \frac{1}{[n(T) + 1]2w(T)\sin^2(\theta + \theta')} \qquad [13]$$

with

$$h(T) = n(T)w(T)\sin^2(\theta + \theta'). \qquad [14]$$

The calculation gives the result that the effective relaxation time of the main line is independent of the nuclear transition while the effective relaxation times of satellite lines are affected by this transition, leading to relaxation $[n(T) + 1]$ times faster. Thus, the G_s/G_m obtained from Eq. [5] and Eq. [6] is given as

$$\frac{G_s}{G_m} = 2(n(T) + 1) \qquad [15]$$

and can reach values larger than a factor 2 where the possible anomalous behavior is proportional to a nuclear transition probability. Since for the more quantitative calculation, a temperature dependance of a transition probability for the main line is also required, the evaluation of all unknown constants from fitting data in Fig. 4 is not possible. However, one can use a convenient transformation to the obtained functional dependence of $w(T)$ and $h(T)$ on G_s and G_m and estimate the expected temperature dependance for these transition probabilities. After a small readjustment of the data, one obtains

$$w(T) \propto \frac{1}{G_m(T)} = w_0(T) \qquad [16]$$

$$h(T) \propto \frac{1}{G_m(T)}\left(\frac{1}{2}\frac{G_m(T)}{G_s(T)} - 1\right) = h_0(T). \qquad [17]$$

Equation [17] was employed for the new presentation of the experimental data by using data in Fig. 5. The data obtained are directly proportional to transition probability and they are shown in Fig. 6. The temperature dependence of the transition probability, which is proportional to the nuclear transition probability, clearly shows a peak around 220 K. The data for $h_0(T)$ can be easily fitted to the functional form in Eq. [11] with an Arrhenius-type correlation time τ, and the fitting curve is shown as a continuous line in Fig. 6. From the fitting procedure, one obtains parameters for the activation energy of the proton-hopping process $\Delta E = 0.22 \pm 0.01$ eV, preexponential constant $\tau_0 = 1.2 \pm 0.7 \times 10^{-13}$ s, and proportionality constant $h_0 = 5.50 \pm 0.09 \times 10^{10}$ mW s^{-1}. These data are in good agreement (within experimental error) with earlier measured τ values for proton hopping which was evaluated from superhyperfine proton splitting. Moreover, the data evaluated in the fitting procedure show better precision than previously obtained data (*21, 22, 25*). The increase in precision can be explained by the larger temperature interval (150–330 K) where the data were obtained, compared to the earlier measurement.

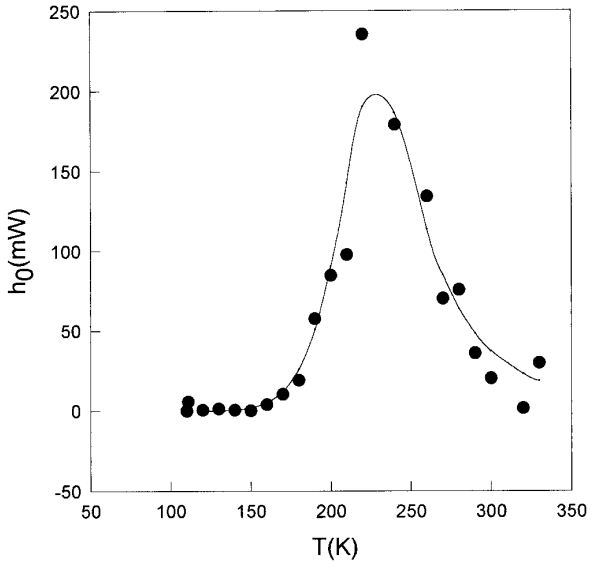

FIG. 6. Temperature dependence of the parameter h_0 obtained from experimental data by employing Eq. [17]. The solid line represents the best fit of h_0 to the temperature-dependent relation, Eq. [11].

The anomalous saturation behavior of J_s/J_m can be explained by introducing an additional END relaxation mechanism. It was demonstrated that significant extreme decrease of a proton spin–lattice relaxation time is responsible for this effect. However, some additional experimental evidence for the END relaxation mechanism can be seen not only around T^* but also in the vicinity of T_C. In the earlier ENDOR experiment (*8*), it was noted that the intensity of proton lines, as well as of potassium and phosphorus lines, rapidly decreases in the paraelectric phase. Since the ENDOR intensity is directly proportional to the nuclear relaxation time, one can assume that an END relaxation mechanism, which exponentially increases with temperature, is

also responsible for the disappearance of ENDOR lines. In order to better examine this assumption, an ENDOR procedure for determining cross-relaxation rates developed by Brustolon and co-workers (*30*) could be also employed by measuring the intensity ratio between ENDOR lines. Our preliminary measurements of T_1 by the DMESR technique show (*31, 32*) a smaller relaxation rate than measured earlier (*3*) and a significant angular dependance of this rate in the vicinity of T_C. These observations indicate a detectable amount of the END relaxation mechanism even in the low-temperature region with reduced motional dynamics. Since the END relaxation mechanism exhibits exponential temperature dependences, it can be also related to the well-examined effect of exponential broadening (*6–8*), whose microscopic origin is not quite clear at higher temperatures ($\sim T^*$).

CONCLUSIONS

In conclusion, the ESR data indicate that, in the hydrogen-bonding ferroelectric lattice, an important contribution to the spin–lattice relaxation rate can arise from the END relaxation mechanism. To our knowledge, besides several earlier obtained experimental data which can be used to partially support an END microscopic relaxation mechanism, these saturation data on forbidden and allowed ESR transitions give the first firm evidence for an END relaxation mechanism which is involved in the relaxation rate of the AsO_4^{4-} center in KDA. By estimating an effective proton distance in O–H$\cdots$O bonds, the earlier proposed model for spontaneous polarization (*28, 29*) which includes charge inbalance in the P–O (As–O) bonds was supported.

ACKNOWLEDGMENTS

The authors thank Professor N. S. Dalal for kindly providing KH_2AsO_4 crystals. The financial support of the Ministry of Science and Technology of the Republic of Croatia is acknowledged.

REFERENCES

1. N. S. Dalal, *Adv. Magn. Reson.* **10,** 119 (1982).
2. K. A. Müller, *Ferroelectrics* **72,** 273 (1987).
3. U. Weisensee, G. Vlkel, and W. Bruner, *Solid State Commun.* **48,** 309 (1983).
4. D. D. Wheeler, H. A. Farach, C. P. Poole, Jr., and R. J. Creswick, *Phys. Rev. B* **37,** 9703 (1988).
5. W. N. Lawless, *Ferroelectrics* **71,** 149 (1987).
6. N. S. Dalal and B. Rakvin, *J. Chem. Phys.* **90,** 5262 (1989).
7. B. Rakvin and N. S. Dalal, *Phys. Rev. B* **41,** 608 (1990).
8. B. Rakvin and N. S. Dalal, *Phys. Rev. B* **44,** 892 (1991).
9. B. Rakvin and N. S. Dalal, *J. Phys. Chem. Solids* **57,** 1483 (1996).
10. W. N. Lawless and V. H. Schmidt, *Jpn. J. Appl. Phys. Suppl.* **24**(2), 952 (1985).
11. L. Kevan and R. N. Schwartz, ''Time Domain ESR,'' Wiley, New York, 1979.
12. R. Blinc, *J. Chem. Solids* **13,** 204 (1966).
13. M. Tokunaga and T. Matsubara, *Prog. Theor. Phys.* **35,** 81 (1966).
14. Y. Tominaga, M. Tokunaga, and I. Tatsuzaki, *Solid State Commun.* **54,** 979 (1985).
15. C. P. Poole, Jr., and H. A. Farach, ''The Theory of Magnetic Resonance,'' Wiley, New York, 1972.
16. D. S. Leniart, J. S. Hyde, and J. C. Vedrine, *J. Phys. Chem.* **76,** 2079 (1972).
17. M. Brustolon and T. Cassol, *J. Magn. Reson.* **60,** 257 (1984).
18. H. Shimizu, *J. Chem. Phys.* **42,** 3603 (1965).
19. R. Blinc, P. Cevc, and M. Schara, *Phys. Rev.* **159,** 411 (1967).
20. N. S. Dalal, C. A. McDowell, and R. Srinivsan, *Mol. Phys.* **24,** 417 (1972).
21. N. S. Dalal and A. C. McDowell, *Phys. Rev. B* **5,** 1074 (1972).
22. B. Lamotte, J. Gaillrad, and O. Constantinescu, *J. Chem. Phys.* **57,** 3319 (1972).
23. G. M. Rebiero, L. V. Gonzaga, A. S. Chaves, R. Gazzinelli, R. Blinc, P. Cevc, P. Prelovšek, and N. I. Silkin, *Phys. Rev. B* **35,** 311 (1982).
24. N. S. Dalal, R. Blinc, P. Prelovek, and A. H. Reddock, *Solid State Commun.* **43,** 887 (1982).
25. B. Rakvin and N. S. Dalal, *Phys. Rev. B* **39,** 7009 (1989).
26. D. H. W. Dickson and A. R. Ubbelohde, *Acta Crystallogr.* **3,** 6 (1950).
27. R. J. Nelmes, Z. Tun, and W. H. Kuhs, *Ferroelectrics* **71,** 125 (1987).
28. B. Rakvin and N. S. Dalal, *Ferroelectrics* **135,** 227 (1996).
29. B. Ravkin and N. S. Dalal, *Solid State Commun.* **92,** 909 (1994).
30. M. Brustolon, T. Cassol, L. Micheletti, and U. Segre, *Mol. Phys.* **57,** 1005 (1986).
31. B. Rakvin, *J. Magn. Reson. A* **106,** 245 (1994).
32. B. Rakvin and N. S. Dalal, *Phys. Rev. B* **49,** 13221 (1994).